

Supporting Information for

Synergistic Oxygen Atom Transfer by the Ruthenium Complexes with Non-redox Metal Ions

Zhanao Lv, Wenrui Zheng, Zhuqi Chen*, Zhiming Tang, Wanling Mo, Guochuan Yin*

School of Chemistry and Chemical Engineering, Key laboratory of Material Chemistry for Energy Conversion and Storage (Huazhong University of Science and Technology), Ministry of Education, Hubei Key Laboratory of Material Chemistry and Service Failure, Huazhong University of Science and Technology, Wuhan 430074, PR China

Email: zqchen@hust.edu.cn, gyin@hust.edu.cn

- Table S1. Influence of the different solvent on the catalytic oxidation of cyclooctene.
Table S2. Influence of the different temperature on the catalytic oxidation of cyclooctene.
Table S3. Influence of the extra ligand on the catalytic oxidation of cyclooctene.
Figure S1. ^1H NMR spectra of $\text{Ru}(\text{bpy})_2\text{Cl}_2$.
Figure S2. ^1H NMR spectra of compound 4 (blue dimer).
Figure S3. ^1H NMR, ^{13}C NMR and ^1H - ^{13}C HSQC spectra of Compound 3.
Figure S4. ^1H NMR spectra of high valent ruthenium with different ratio of $\text{Al}(\text{OTf})_3$.
Table S4. ^1H NMR chemical shifts of the different compounds.
Figure S5. GC-MS graph of catalytic epoxidation of cyclooctene.
Figure S6. GC-MS graph of H_2^{18}O labeled catalytic *cis*-stilbene epoxidation.
Table S5. Crystal data and structure refinement for $\text{Ru}^{\text{III}}(\text{C}_{10}\text{H}_8\text{N}_2)_2(\text{CF}_3\text{SO}_3)\text{Cl}_2 \cdot \text{CH}_3\text{CN}$.
Figure S7. The structure of $\text{Ru}^{\text{III}}(\text{C}_{10}\text{H}_8\text{N}_2)_2(\text{CF}_3\text{SO}_3)\text{Cl}_2$.
Figure S8. Packing diagram for $\text{Ru}^{\text{III}}(\text{C}_{10}\text{H}_8\text{N}_2)_2(\text{CF}_3\text{SO}_3)\text{Cl}_2 \cdot \text{CH}_3\text{CN}$.
Table S6. Atomic coordinates and equivalent isotropic displacement parameters for $\text{Ru}^{\text{III}}(\text{C}_{10}\text{H}_8\text{N}_2)_2(\text{CF}_3\text{SO}_3)\text{Cl}_2 \cdot \text{CH}_3\text{CN}$.
Table S7. Selected Bond Distances and Angles for $\text{Ru}^{\text{III}}(\text{C}_{10}\text{H}_8\text{N}_2)_2(\text{CF}_3\text{SO}_3)\text{Cl}_2 \cdot \text{CH}_3\text{CN}$.
Table S8. Anisotropic displacement parameters for $\text{Ru}^{\text{III}}(\text{C}_{10}\text{H}_8\text{N}_2)_2(\text{CF}_3\text{SO}_3)\text{Cl}_2 \cdot \text{CH}_3\text{CN}$.
Table S9. Hydrogen coordinates and isotropic displacement parameters for $\text{Ru}^{\text{III}}(\text{C}_{10}\text{H}_8\text{N}_2)_2(\text{CF}_3\text{SO}_3)\text{Cl}_2 \cdot \text{CH}_3\text{CN}$.
Figure S9. UV-Vis absorption spectra of Compound 2, Compound 3 and their mixture with 1:1 ratio.
Table S10. Catalytic oxidation of cyclooctene by $\text{Ru}(\text{bpy})_2\text{Cl}_2$ and $\text{Al}(\text{OTf})_3$ in dark.
Table S11 Catalytic oxidation of cyclooctene by $\text{Ru}(\text{bpy})_2\text{Cl}_2$ and $\text{Al}(\text{OTf})_3$ with different oxidant
Table S12 Influence of water concentration on the epoxidation of *cis*-stilbene by $\text{Ru}(\text{bpy})_2\text{Cl}_2$ and $\text{Al}(\text{OTf})_3$
Table S13. Catalytic oxidation of cyclooctene by $\text{Ru}(\text{bpy})_2\text{Cl}_2$ and $\text{Al}(\text{OTf})_3$ under O_2 or Ar.

Table S1. Influence of the different solvent on the catalytic oxidation of cyclooctene to 1,2-epoxycyclooctane.

CH ₂ Cl ₂	CH ₃ COCH ₃	Conversion (%)	Yield (%)
4	1	74.9	52.2
3	2	91.5	55.6
2	3	95.4	63.9
1	4	99.9	89.9

Conditions: solvent 1 mL, cyclooctene 0.1 M, *cis*-Ru(bpy)₂Cl₂ 1 mM, 2,2'-bipyridine 2 mM, Al(OTf)₃ 2 mM, PhI(OAc)₂ 0.2 M, 308 K, 10 h.

Table S2. Influence of the different temperature on the catalytic oxidation of cyclooctene to 1,2-epoxycyclooctane.

Entry	T	Conversion (%)	Yield (%)
1	303K	56.1	35.6
2	308k	99.9	89.9
3	313k	99.6	68.4

Conditions: solvent acetone 0.8 mL CH₂Cl₂ 0.2 mL, cyclooctene 0.1 M, *cis*-Ru(bpy)₂Cl₂ 1 mM, 2,2'-bipyridine 2 mM, Al(OTf)₃ 2 mM, PhI(OAc)₂ 0.2 M, 10 h.

Table S3 Influence of the extra ligand on the catalytic oxidation of cyclooctene to 1,2- epoxycyclooctane.

Entry	Catalyst	Lewis acid	Additives	Conversion (%)	Yield (%)
1	RuCl ₃	-	-	32.2	7.0
2	RuCl ₃	Al(OTf) ₃	-	99.6	32.6
3	RuCl ₃	Al(OTf) ₃	2,2'-bipyridine (6 mM)	100.0	70.1
4	Ru(bpy) ₂ Cl ₂	Al(OTf) ₃	-	99.1	67.9
5	Ru(bpy) ₂ Cl ₂	Al(OTf) ₃	2,2'-bipyridine (2 mM)	99.9	89.9

Conditions: acetone/CH₂Cl₂ (4:1, v/v) 1 mL, cyclooctene 0.1 M, ruthenium catalyst 1 mM, Al(OTf)₃ 2 mM, PhI(OAc)₂ 0.2 M, 308K, 10 h.

Cis-Dichloro-bis-(bipyridine) ruthenium: Ru(bpy)₂Cl₂

In a typical reaction RuCl₃ (0.4 g, 1.91 mmol), lithium chloride (0.55 g, 13.00 mmol) and 2,2'-bipyridine (0.59 g, 3.82 mmol) were dissolved in anhydrous DMF (7 mL). The mixture was heated at reflux under a nitrogen environment at 160 °C for 8 h. At this time the reaction mixture was allowed to reach room temperature and acetone (25 ml) was added. The solution was placed at -20 °C overnight and the resulting black precipitate filtered. The precipitate was washed well with acetone and diethyl ether to leave a dark purple colored solid. The product was purified on a silica chromatographic column using 10 % methanol-dichloromethane as mobile phase. The material was lyophilized to yield the product as a dark purple solid. Typical yield: 60-65 %.

¹H NMR (400 MHz, DMSO-d₆) δ 9.98 (dd, J = 5.8, 1.5 Hz, 2H), 8.66 (d, J = 8.1 Hz, 2H), 8.50 (d, J = 8.0 Hz, 2H), 8.08 (td, J = 7.8, 1.6 Hz, 2H), 7.79 (ddd, J = 7.3, 5.7, 1.3 Hz, 2H), 7.69 (td, J = 7.8, 1.5 Hz, 2H), 7.52 (dd, J = 6.0, 1.4 Hz, 2H), 7.12 (ddd, J = 7.3, 5.7, 1.4 Hz, 2H).

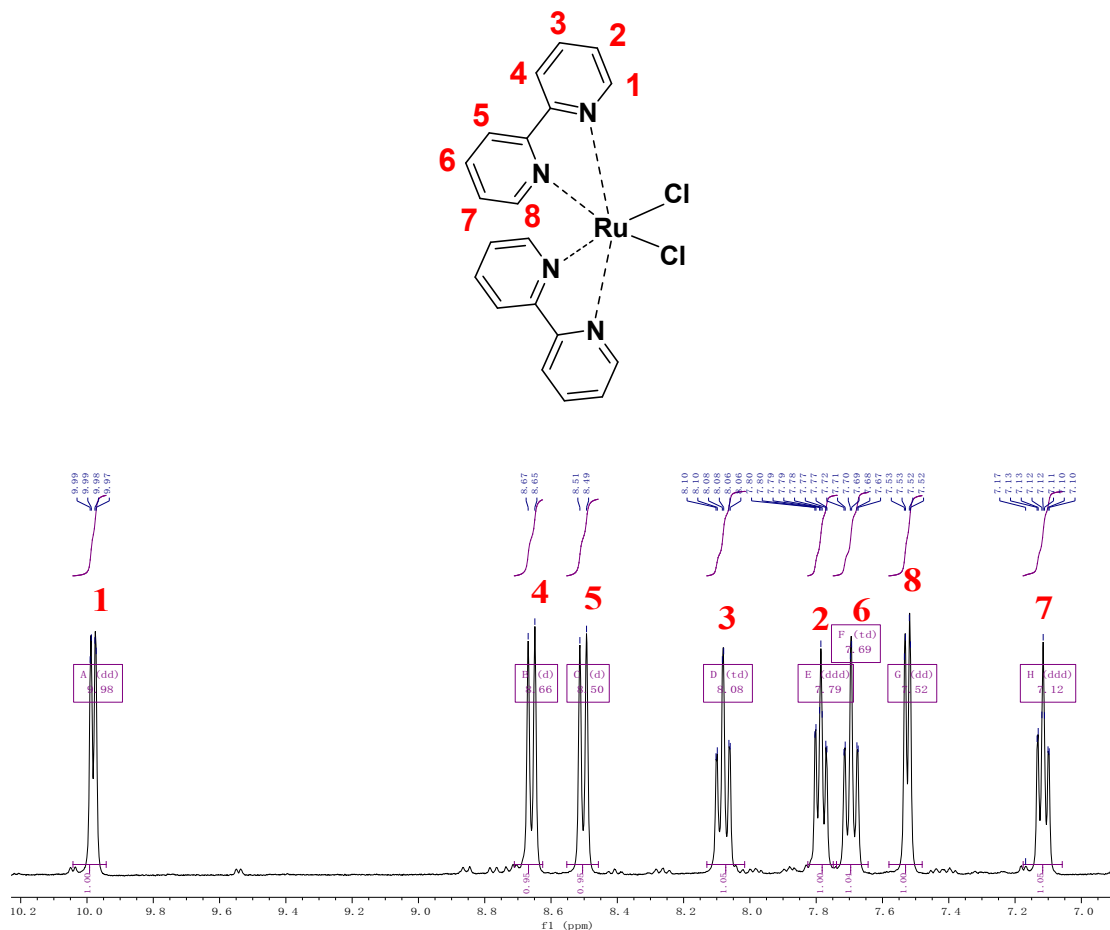


Figure S1. ^1H NMR spectra of $\text{Ru}(\text{bpy})_2\text{Cl}_2$.

Compound 4

^1H NMR (400 MHz, DMSO-d_6) δ 10.21 (dd, $J = 5.6, 1.4$ Hz, 2H), 9.67 (d, $J = 8.1$ Hz, 2H), 9.53 (d, $J = 8.1$ Hz, 2H), 9.20 (td, $J = 7.9, 1.5$ Hz, 2H), 8.88 (td, $J = 7.9, 1.5$ Hz, 2H), 8.77 (ddd, $J = 7.3, 5.6, 1.2$ Hz, 2H), 8.42 (dd, $J = 5.7, 1.3$ Hz, 2H), 8.22 (ddd, $J = 7.2, 5.7, 1.2$ Hz, 2H).

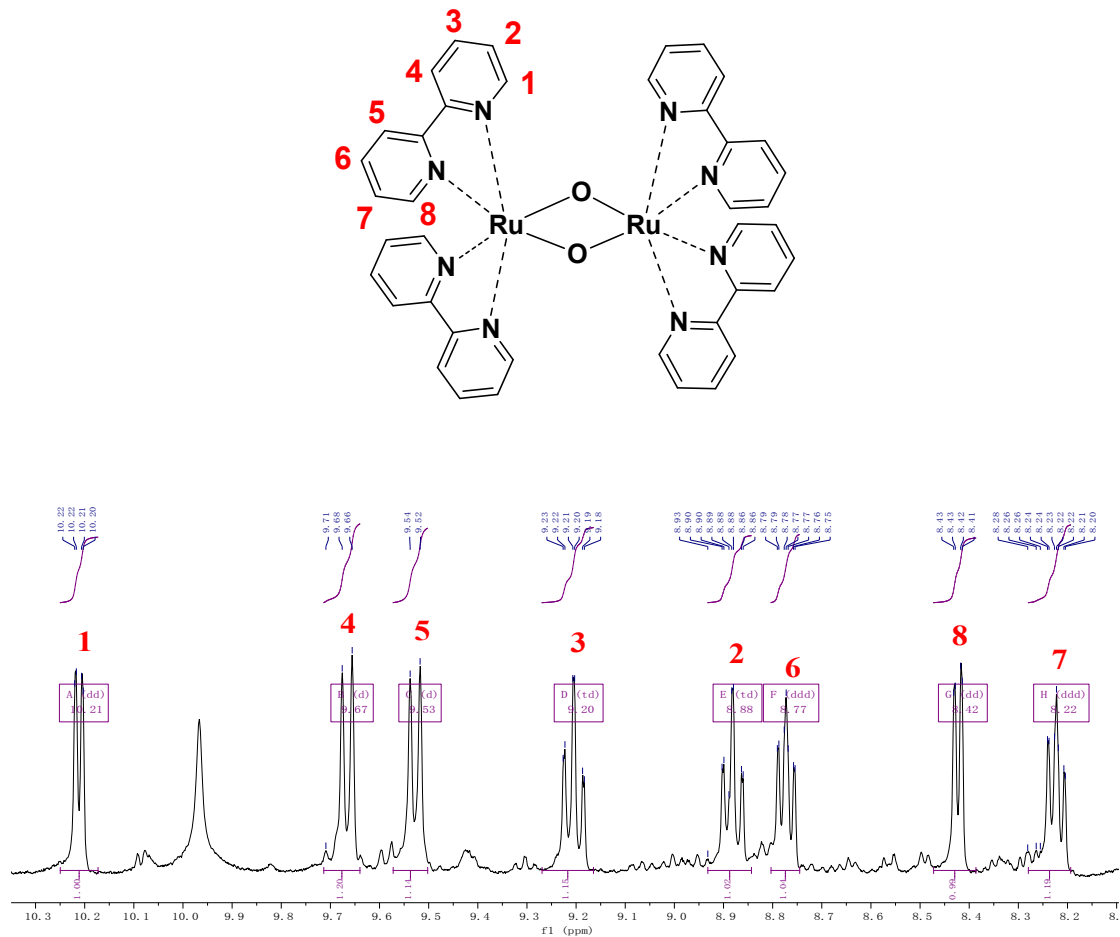


Figure S2. ^1H NMR spectra of compound 4 (blue dimer).

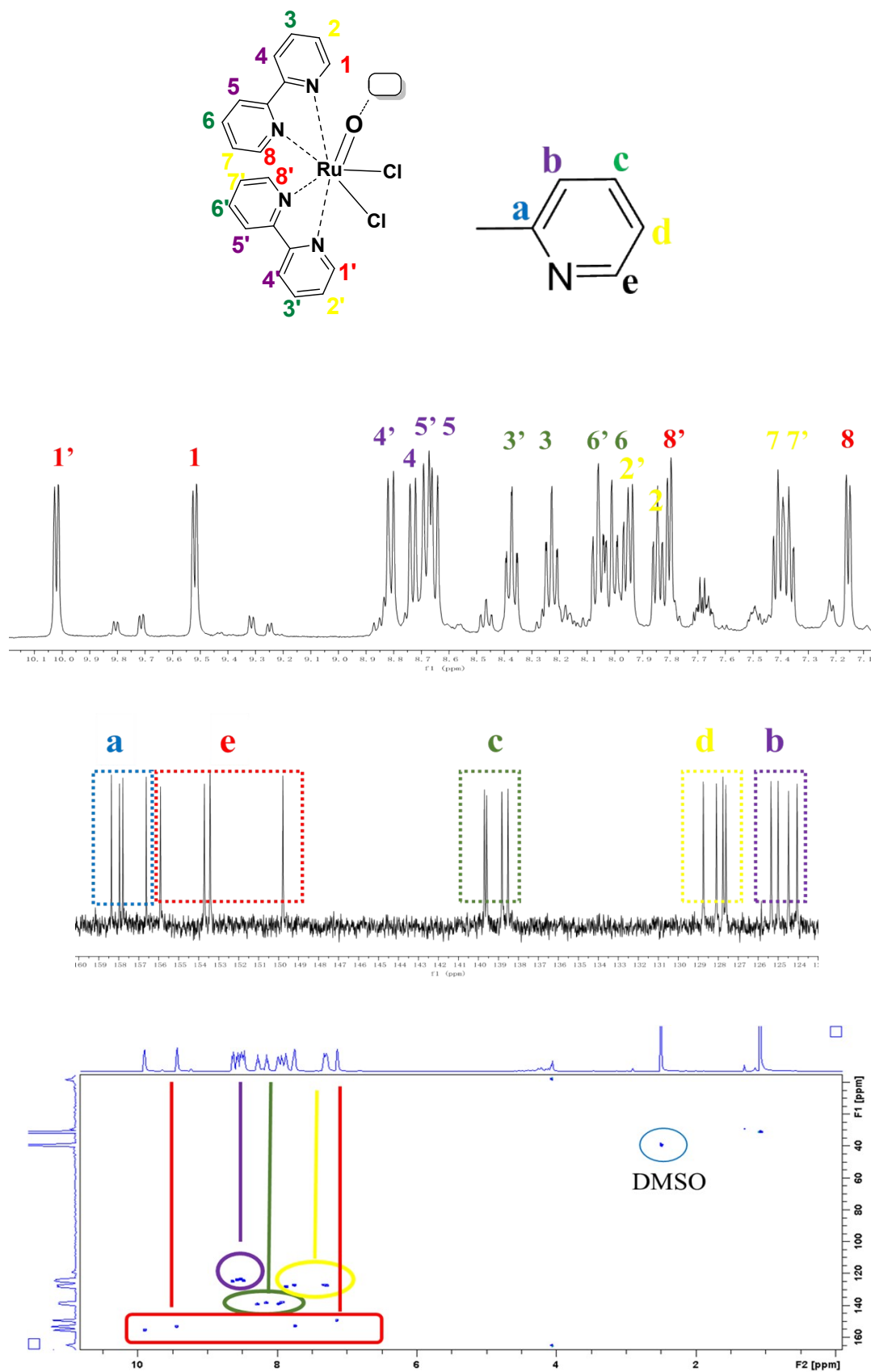


Figure S3. ^1H NMR, ^{13}C NMR and ^1H - ^{13}C HSQC spectra of Compound 3.

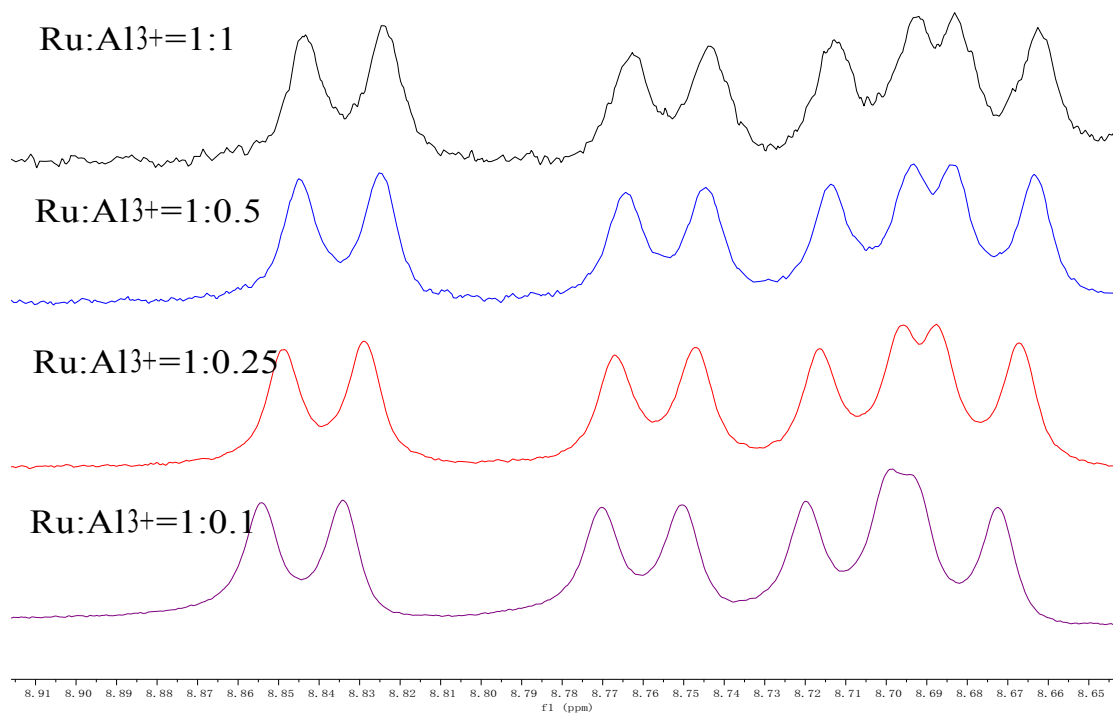
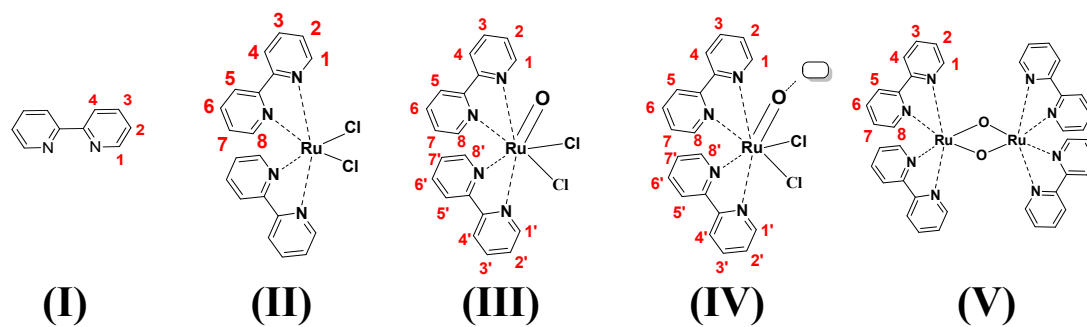


Figure S4. ^1H NMR spectra of high valent ruthenium with different ratio of $\text{Al}(\text{OTf})_3$.

Table S4. ^1H NMR chemical shifts (in ppm relative to TMS) of the different compounds.



Compound	H1(1')	H2(2')	H3(3')	H4(4')	H5(5')	H6(6')	H7(7')	H8(8')
I	8.40	7.47	7.96	8.70				
II	9.98	7.79	8.08	8.66	8.50	7.69	7.12	7.52
III	9.53 (10.03)	7.87 (7.97)	8.25 (8.40)	8.76 (8.85)	8.70	8.03 (8.08)	7.41	7.17 (7.82)
IV	9.52 (10.02)	7.85 (7.95)	8.23 (8.37)	8.73 (8.81)	8.67	8.01 (8.06)	7.39	7.16 (7.80)
V	10.21	8.88	9.20	9.67	9.53	8.77	8.22	8.42

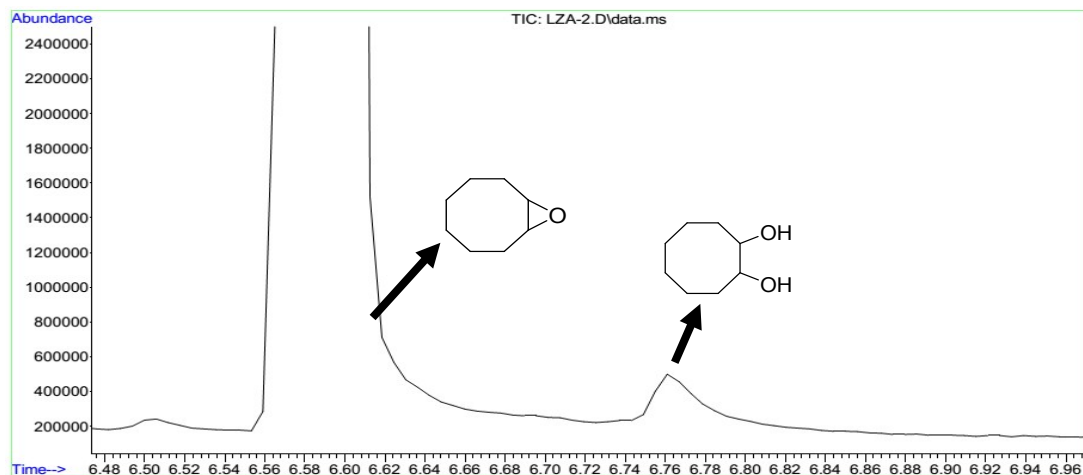


Figure S5. Enlarged GC-MS graph of catalytic epoxidation of cyclooctene by $\text{Ru}(\text{bpy})_2\text{Cl}_2$ and $\text{Al}(\text{OTf})_3$ to illustrate trace 1,2-cyclooctanediol product. Conditions: CH_3COCH_3 0.8 mL, CH_2Cl_2 0.2 mL, 1,2-cyclooctene 0.1 M, *cis*- $\text{Ru}(\text{bpy})_2\text{Cl}_2$ 1 mM, 2,2'-bipyridine 2 mM, $\text{Al}(\text{OTf})_3$ 2 mM, $\text{PhI}(\text{OAc})_2$ 0.2 M, 308 K, 10 h.

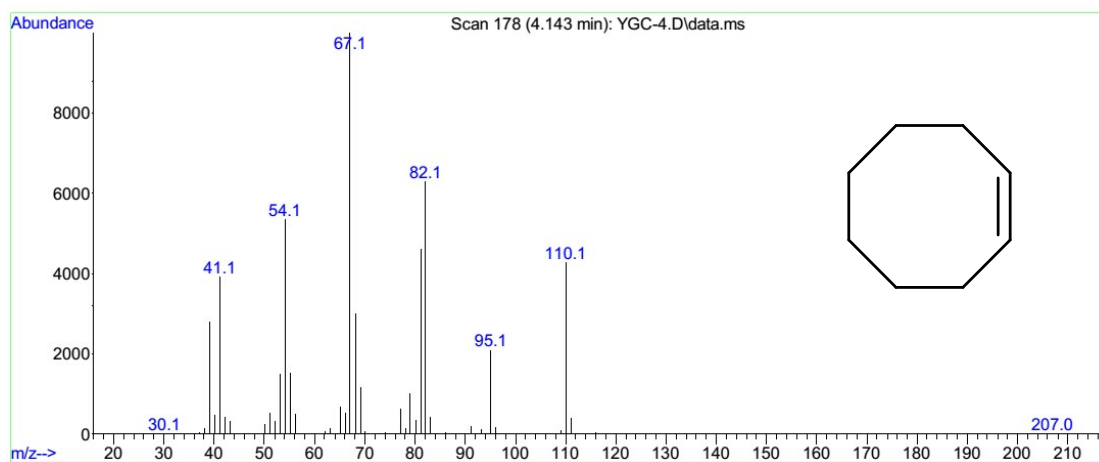


Figure S5-1. MS graph of cyclooctene from catalytic epoxidation of cyclooctene by *cis*- $\text{Ru}(\text{bpy})_2\text{Cl}_2$ and $\text{Al}(\text{OTf})_3$.

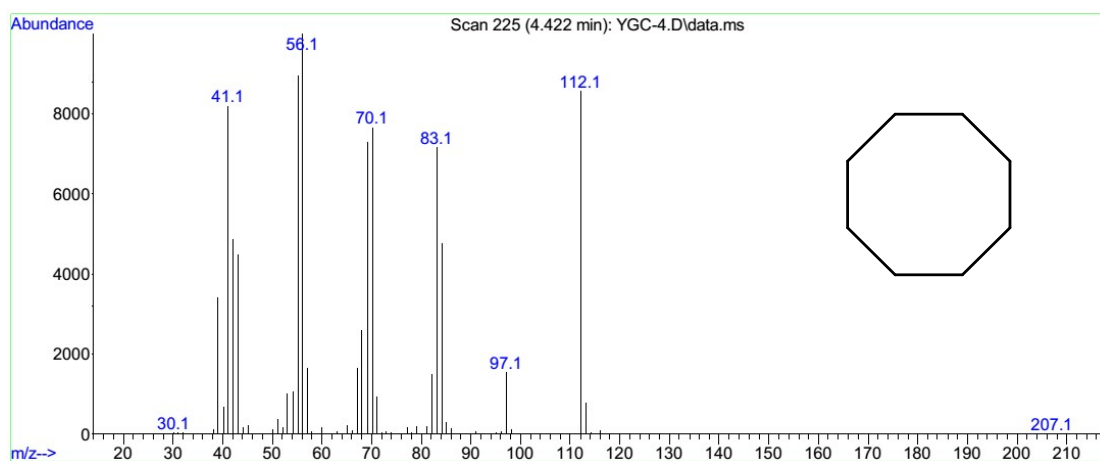


Figure S5-2. MS graph of cyclooctane from catalytic epoxidation of cyclooctene by *cis*-Ru(bpy)₂Cl₂ and Al(OTf)₃.

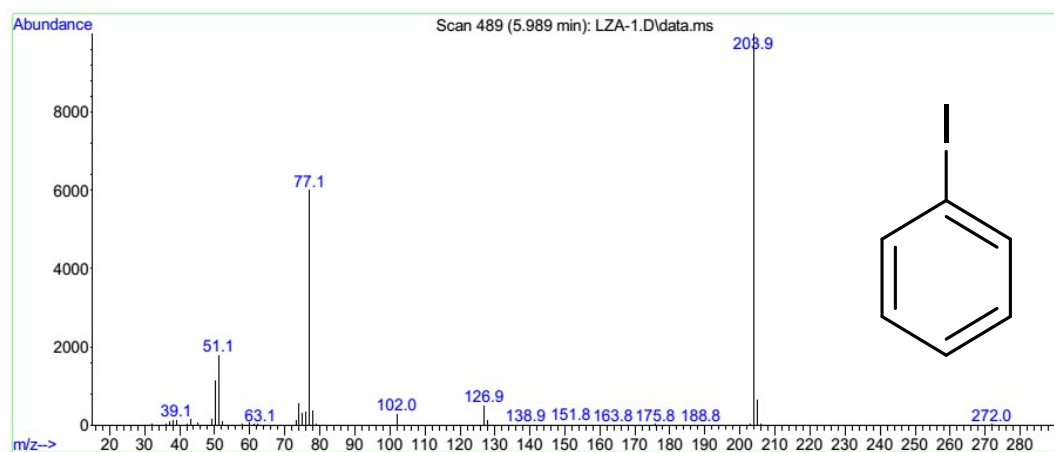


Figure S5-3. MS graph of iodobenzene from catalytic epoxidation of cyclooctene by *cis*-Ru(bpy)₂Cl₂ and Al(OTf)₃.

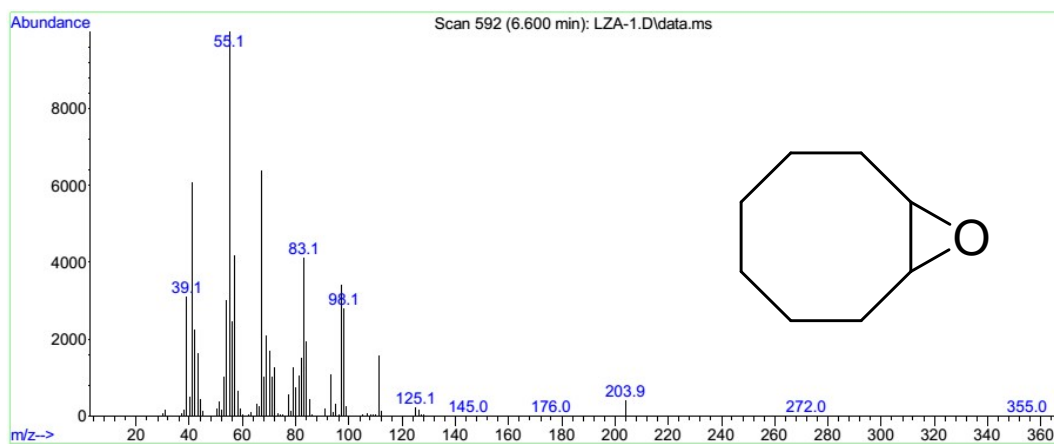


Figure S5-4. MS graph of 1,2-epoxycyclooctane from catalytic epoxidation of cyclooctene by *cis*-Ru(bpy)₂Cl₂ and Al(OTf)₃.

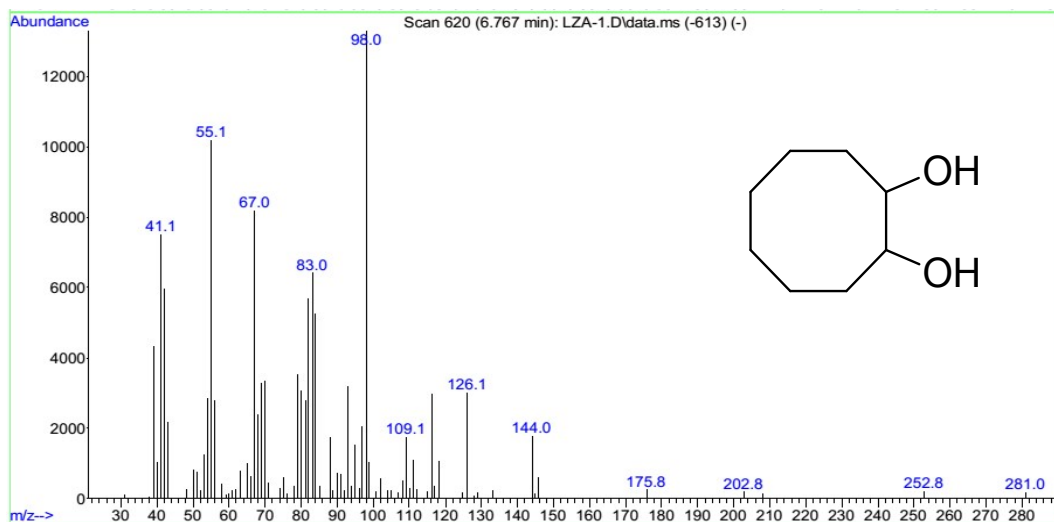


Figure S5-5. MS graph of 1,2-cyclooctanediol from catalytic epoxidation of cyclooctene by *cis*-Ru(bpy)₂Cl₂ and Al(OTf)₃.

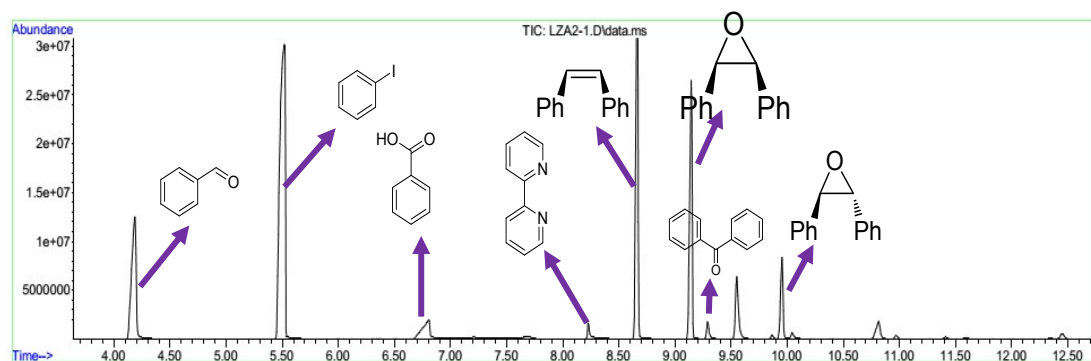


Figure S6. GC-MS graph of H_2^{18}O labeled catalytic *cis*-stilbene epoxidation by the ruthenium(II) complex and $\text{Al}(\text{OTf})_3$. Conditions: H_2^{18}O 0.1 mL, acetone 0.8 mL, CH_2Cl_2 0.2 mL, *cis*-stilbene 0.1 M, *cis*- $\text{Ru}(\text{bpy})_2\text{Cl}_2$ 1 mM, 2,2'-bipyridine 2 mM, $\text{Al}(\text{OTf})_3$ 2 mM, $\text{PhI}(\text{OAc})_2$ 0.2 M, 298 K, 12 h.

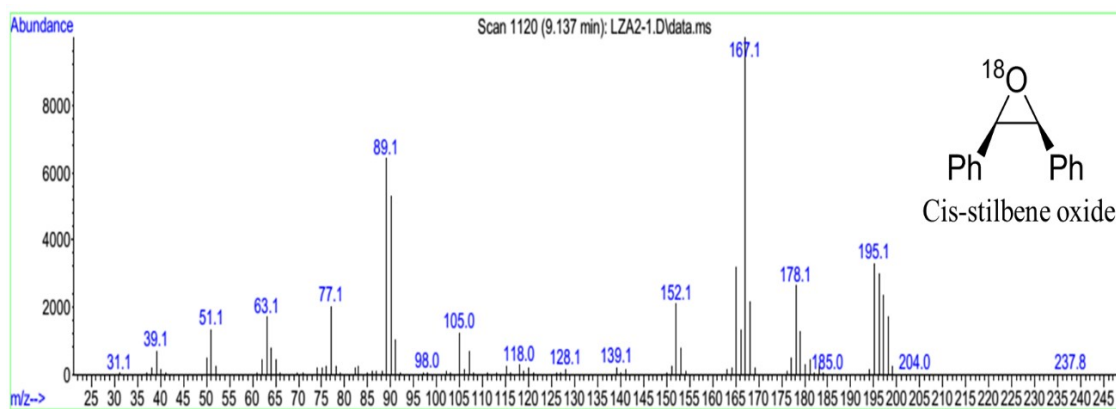


Figure S6-1. MS graph of ^{18}O labeled *cis*-stilbene oxide from catalytic epoxidation of *cis*-stilbene by *cis*- $\text{Ru}(\text{bpy})_2\text{Cl}_2$ and $\text{Al}(\text{OTf})_3$.

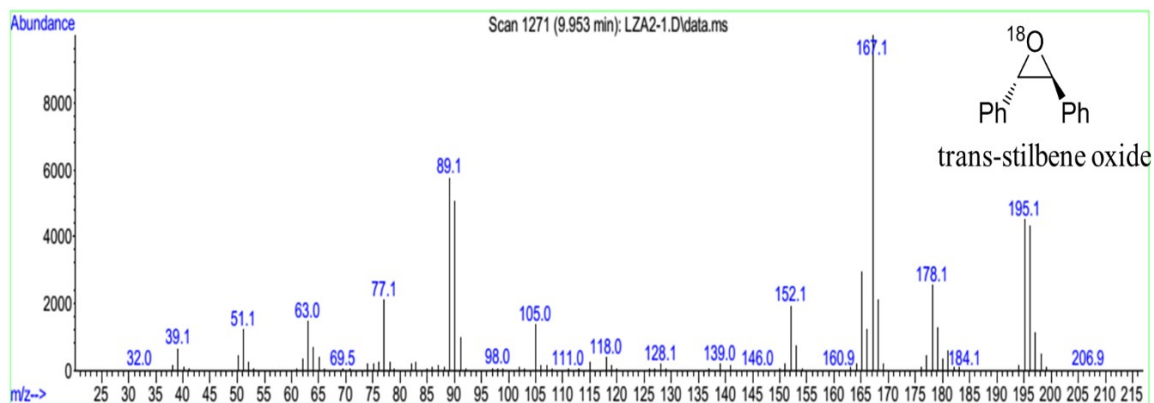


Figure S6-2. MS graph of ^{18}O labeled *trans*-stilbene oxide from catalytic epoxidation of *cis*-stilbene by *cis*- $\text{Ru}(\text{bpy})_2\text{Cl}_2$ and $\text{Al}(\text{OTf})_3$.

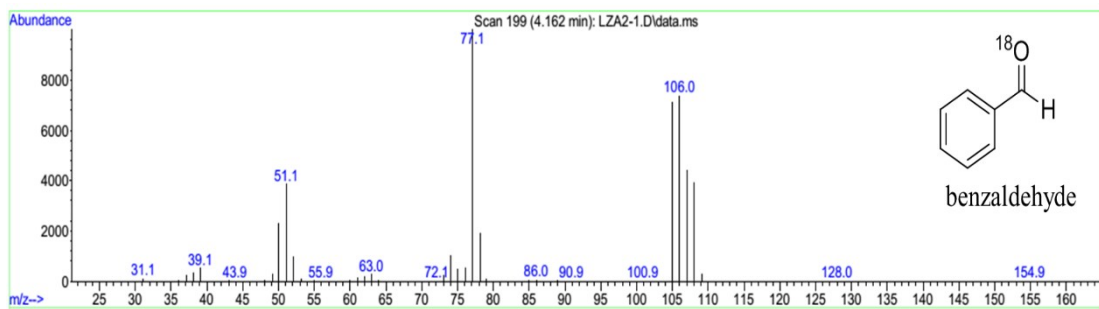


Figure S6-3. MS graph of ^{18}O labeled benzaldehyde from catalytic epoxidation of *cis*-stilbene by *cis*- $\text{Ru}(\text{bpy})_2\text{Cl}_2$ and $\text{Al}(\text{OTf})_3$.

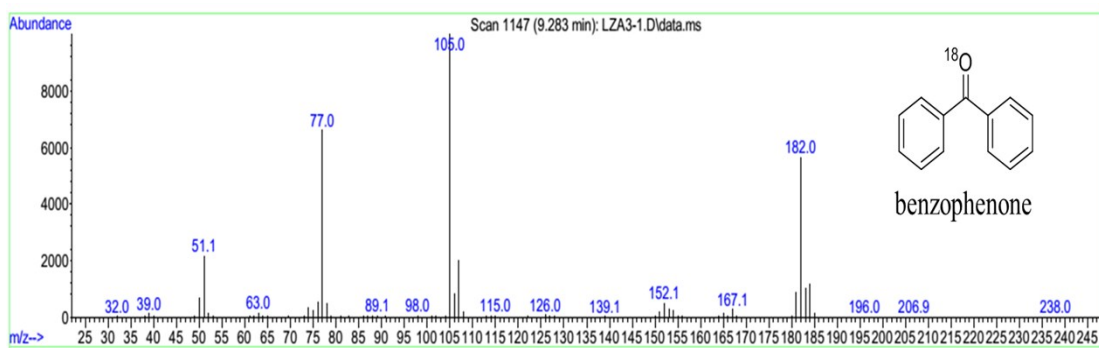


Figure S6-4. MS graph of ^{18}O labeled benzophenone from catalytic epoxidation of *cis*-stilbene by *cis*- $\text{Ru}(\text{bpy})_2\text{Cl}_2$ and $\text{Al}(\text{OTf})_3$.

Table S5. Crystal data and structure refinement for Ru^{III}(C₁₀H₈N₂)₂(CF₃SO₃)Cl₂·CH₃CN.

Identification code	1411258	
Empirical formula	C ₂₃ H ₁₉ Cl ₂ F ₃ N ₅ O ₃ RuS	
Formula weight	674.46	
Temperature	173(2) K	
Wavelength	0.71073 Å	
Crystal system	Monoclinic	
Space group	Cc	
Unit cell dimensions	a = 15.0950(6) Å	α = 90.00°.
	b = 14.0023(6) Å	β = 108.6890(10)°.
	c = 12.3350(5) Å	γ = 90.00°.
Volume	2469.71(18) Å ³	
Z	4	
Density (calculated)	1.811 Mg/m ³	
Absorption coefficient	0.999 mm ⁻¹	
F(000)	1336	
Crystal colour and habit	Orange block	
Crystal size	0.25 x 0.17 x 0.14 mm ³	
Theta range for data collection	3.39 to 30.56°.	
Index ranges	-21 ≤ h ≤ 12, -19 ≤ k ≤ 20, -17 ≤ l ≤ 17	
Reflections collected	13139	
Independent reflections	5534 [R(int) = 0.0194]	
Completeness to theta = 30.56°	99.4 %	
Absorption correction	multi-scan	
Max. and min. transmission	0.871 and 0.813	
Refinement method	Full-matrix least-squares on F ²	
Data / restraints / parameters	5534 / 2 / 345	
Goodness-of-fit on F ²	1.031	
Final R indices [I > 2σ(I)]	R1 = 0.0217, wR2 = 0.0539	
R indices (all data)	R1 = 0.0231, wR2 = 0.0548	
Largest diff. peak and hole	0.391 and -0.374 e.Å ⁻³	

Definitions:

$$R_1 = \frac{\sum \|F_o\| - \|F_c\|}{\sum \|F_o\|} \quad wR_2 = \sqrt{\frac{\sum [w(F_o^2 - F_c^2)^2]}{\sum [w(F_o^2)^2]}}$$

$$Goof = \sqrt{\frac{\sum [w(F_o^2 - F_c^2)]}{(n - p)}}$$

n = number of reflections; p = number of parameters

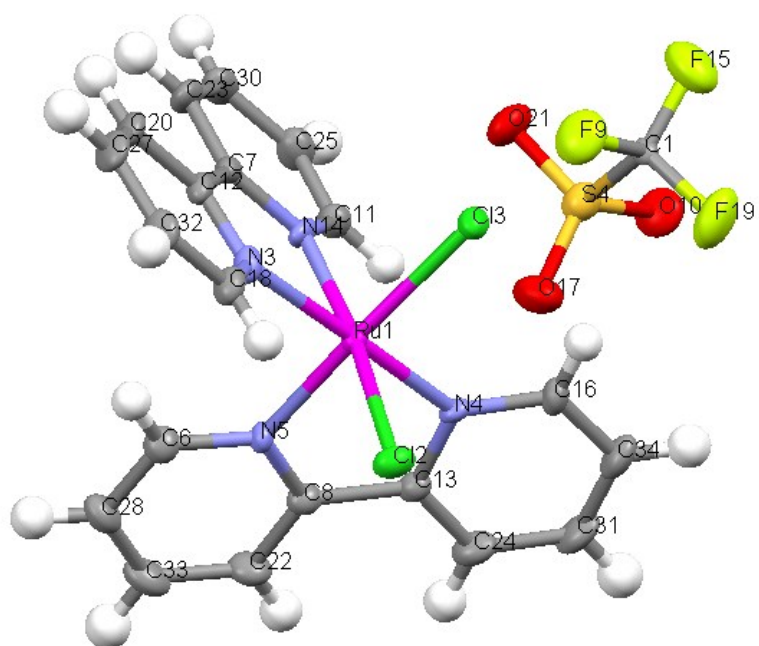


Figure S7. The structure of $\text{Ru}^{\text{III}}(\text{C}_{10}\text{H}_8\text{N}_2)(\text{CF}_3\text{SO}_3)\text{Cl}_2$.

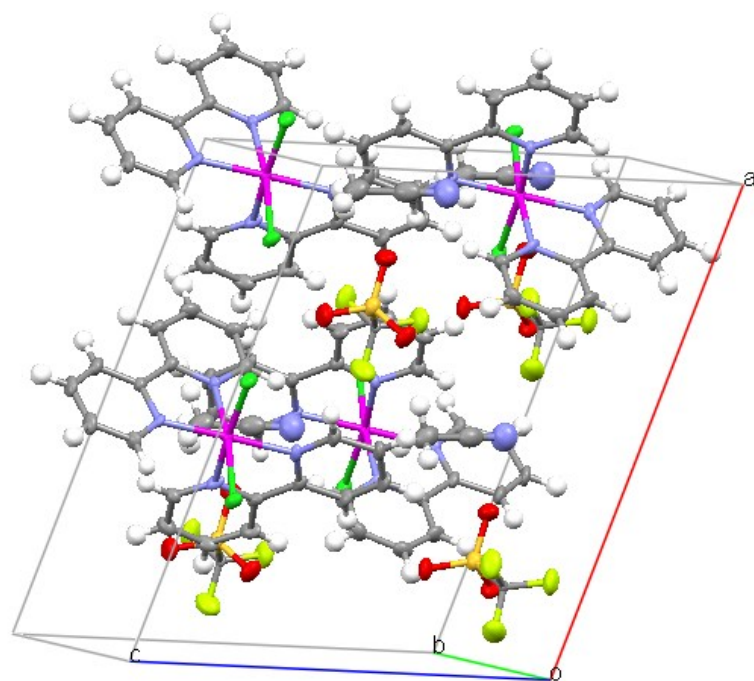


Figure S8. Packing diagram for $\text{Ru}^{\text{III}}(\text{C}_{10}\text{H}_8\text{N}_2)_2(\text{CF}_3\text{SO}_3)\text{Cl}_2 \cdot \text{CH}_3\text{CN}$.

Table S6. Atomic coordinates ($\times 10^4$) and equivalent isotropic displacement parameters ($\text{\AA}^2 \times 10^3$) for $\text{Ru}^{\text{III}}(\text{C}_{10}\text{H}_8\text{N}_2)_2(\text{CF}_3\text{SO}_3)\text{Cl}_2 \cdot \text{CH}_3\text{CN}$. $U(\text{eq})$ is defined as one third of the trace of the orthogonalized U^{ij} tensor.

Atom	x	y	z	U(eq)
Ru1	4456(1)	1852(1)	9186(1)	14(1)
Cl2	5635(1)	704(1)	9553(1)	25(1)
Cl3	3242(1)	723(1)	8813(1)	23(1)
S4	2161(1)	3028(1)	11968(1)	30(1)
N1	-439(5)	-92(4)	11825(5)	66(3)
N3	4192(3)	1926(2)	7429(3)	21(2)
N4	4710(3)	1869(2)	10930(3)	15(1)
N5	5452(2)	2896(2)	9680(2)	17(1)
N14	3492(2)	2949(2)	8752(3)	19(2)
C1	1722(3)	1884(2)	11376(3)	13(2)
C2	-490(3)	-619(3)	13806(3)	48(2)
C6	5785(3)	3388(3)	8951(3)	25(2)
C7	3177(3)	3166(2)	7589(4)	20(2)
C8	5794(3)	3083(2)	10805(4)	20(2)
C9	-460(3)	-323(2)	12686(3)	45(2)
C11	3171(3)	3429(3)	9463(3)	24(2)
C12	3565(3)	2576(2)	6871(3)	21(2)
C13	5395(3)	2488(2)	11526(3)	19(2)
C16	4332(3)	1276(2)	11522(3)	24(1)
C18	4573(3)	1342(3)	6853(3)	25(2)
C20	3302(3)	2651(3)	5672(3)	28(2)
C22	6462(3)	3770(3)	11235(3)	28(2)
C23	2530(3)	3902(3)	7201(4)	29(2)
C24	5710(3)	2505(3)	12705(3)	28(2)
C25	2529(3)	4160(3)	9114(4)	33(2)
C27	3685(3)	2039(3)	5077(3)	32(2)
C28	6468(3)	4081(3)	9334(4)	30(2)
C30	2209(3)	4405(2)	7962(4)	32(2)
C31	5321(4)	1877(3)	13302(4)	33(2)
C32	4335(3)	1380(3)	5668(3)	30(2)
C33	6815(3)	4265(3)	10486(4)	33(2)
C34	4631(3)	1257(3)	12707(3)	31(2)
F9	1872(3)	1723(2)	10364(3)	46(2)
F15	838(2)	1761(2)	11230(3)	54(2)
F19	2195(3)	1170(2)	12095(2)	50(1)
O10	1955(3)	3064(2)	13014(3)	39(2)
O17	3142(2)	2997(2)	12081(3)	42(1)
O21	1620(2)	3681(2)	11109(2)	35(2)

Table S7. Selected Bond Distances [Å] and Angles [°] for Ru^{III}(C₁₀H₈N₂)₂(CF₃SO₃)Cl₂•CH₃CN.

Complex	Ru ^{III} (C ₁₀ H ₈ N ₂) ₂ (CF ₃ SO ₃)Cl ₂	
Ru-Cl lengthes	Cl(2)-Ru(1)	2.332(1)
	Cl(3)-Ru(1)	2.352(1)
Ru-N lengthes	N(5)-Ru(1)	2.044(3)
	N(3)-Ru(1)	2.077(4)
	N(4)-Ru(1)	2.061(4)
	N(14)-Ru(1)	2.065(3)
N-Ru-N angles	N(5)-Ru(1)-N(4)	78.9(1)
	N(5)-Ru(1)-N(14)	86.3(1)
	N(5)-Ru(1)-N(3)	98.8(1)
	N(4)-Ru(1)-N(14)	98.2(1)
	N(4)-Ru(1)-N(3)	176.5(1)
	N(14)-Ru(1)-N(3)	79.0(1)
Cl-Ru-Cl angle	Cl(2)-Ru(1)-Cl(3)	94.2(1)
Cl-Ru-N angles	Cl(2)-Ru(1)-N(5)	89.6(1)
	Cl(3)-Ru(1)-N(5)	172.5(1)
	Cl(2)-Ru(1)-N(4)	86.0(1)
	Cl(3)-Ru(1)-N(4)	94.8(1)
	Cl(2)-Ru(1)-N(14)	173.5(1)
	Cl(3)-Ru(1)-N(14)	90.5(1)
	Cl(2)-Ru(1)-N(3)	96.7(1)
	Cl(3)-Ru(1)-N(3)	87.3(1)

Table S8. Anisotropic displacement parameters ($\text{\AA}^2 \times 10^3$) for $\text{Ru}^{\text{III}}(\text{C}_{10}\text{H}_8\text{N}_2)_2(\text{CF}_3\text{SO}_3)\text{Cl}_2 \cdot \text{CH}_3\text{CN}$.

Atom	U11	U22	U33	U12	U13	U23
Ru1	16.9(1)	14.7(1)	11.2(1)	-0.8(1)	2.8(1)	0.1(1)
Cl2	24(1)	25(1)	25(1)	6(1)	2(1)	-2.2(3)
Cl3	23(1)	24(1)	21(1)	-6(1)	2.0(1)	3(1)
S4	34(1)	31(1)	25(1)	3(1)	8(1)	1.0(3)
N1	74(3)	60(2)	63(3)	-8(2)	24(2)	-1(2)
N3	29(2)	19(1)	16(2)	-6(1)	9(1)	-2(1)
N4	16(2)	19(1)	10(1)	2(1)	0(1)	0(1)
N5	20(1)	17(1)	14(1)	-2(1)	7(1)	3(1)
N14	22(2)	15(1)	21(1)	-2(1)	-2(1)	8.4(1)
C1	16(2)	13(1)	9(1)	-2(1)	5(1)	-4(1)
C2	47(2)	45(2)	51(2)	1(2)	0(2)	-6(1)
C6	29(2)	22(1)	23(2)	0(2)	9(2)	-3(1)
C7	16(2)	25(2)	19(2)	-4(1)	2(1)	7(1)
C8	21(2)	18(1)	20(2)	1(1)	4(1)	-3(1)
C9	38(2)	37(2)	61(2)	1(1)	8(2)	-11(2)
C11	23(2)	24(2)	25(2)	4(2)	9(1)	2(1)
C12	25(2)	23(1)	14(1)	-8(1)	2(1)	3(1)
C13	20(2)	22(1)	16(1)	2(1)	5(1)	-1(1)
C16	29(2)	21(1)	21(2)	0(1)	11(1)	6(1)
C18	33(2)	28(2)	15(2)	-4(2)	7(1)	0(1)
C20	32(2)	36(2)	15(1)	-4(1)	3(1)	8(1)
C22	25(2)	33(2)	26(2)	-6(1)	3(1)	-8(1)
C23	26(2)	28(1)	33(2)	4(1)	3(1)	16(1)
C24	30(2)	38(2)	17(1)	5(1)	2(1)	-5(1)
C25	32(2)	29(2)	39(2)	6(2)	19(2)	4(1)
C27	40(2)	44(2)	12(1)	-5(2)	7(1)	4(1)
C28	26(2)	25(2)	40(2)	-7(1)	13(2)	-2(1)
C30	24(2)	26(1)	45(2)	7(1)	12(1)	12(1)
C31	41(2)	44(2)	14(1)	13(2)	7(1)	4(1)
C32	37(2)	35(2)	18(2)	-7(2)	13(1)	-6(1)
C33	25(2)	28(1)	45(2)	-8(1)	9(2)	-12(1)
C34	44(2)	32(2)	18(2)	10(2)	11(1)	7(1)
F9	63(2)	45(1)	29(1)	2(1)	17(1)	-11(1)
F15	46(2)	60(2)	57(2)	-22(1)	21(1)	-15(1)
F19	80(2)	31(1)	39(1)	12(1)	19(1)	10(1)
O10	50(2)	45(1)	23(1)	3(1)	15(1)	-10(1)
O17	27(1)	61(2)	38(1)	-4(1)	7(1)	-2(1)
O21	43(2)	31(1)	32(1)	8(1)	2(1)	9(1)

Table S9. Hydrogen coordinates ($\times 10^4$) and isotropic displacement parameters ($\text{\AA}^2 \times 10^3$) for $\text{Ru}^{\text{III}}(\text{C}_{10}\text{H}_8\text{N}_2)_2(\text{CF}_3\text{SO}_3)\text{Cl}_2 \cdot \text{CH}_3\text{CN}$.

Atom	x	y	z	U(eq)
H2	5545	3254	8155	30
H2A	141	-790	14294	77
H2B	-904	-1173	13718	77
H2C	-728	-92	14158	77
H11	3391	3265	10252	28
H16	3844	857	11113	28
H18	5022	886	7263	31
H20	2863	3121	5278	35
H22	6679	3906	12032	35
H23	2311	4058	6410	36
H24	6186	2939	13105	35
H25	2310	4490	9652	38
H27	3503	2070	4266	39
H28	6692	4423	8810	36
H30	1774	4911	7701	38
H31	5531	1878	14115	40
H32	4617	957	5273	35
H33	7294	4728	10770	40
H34	4363	821	13103	37

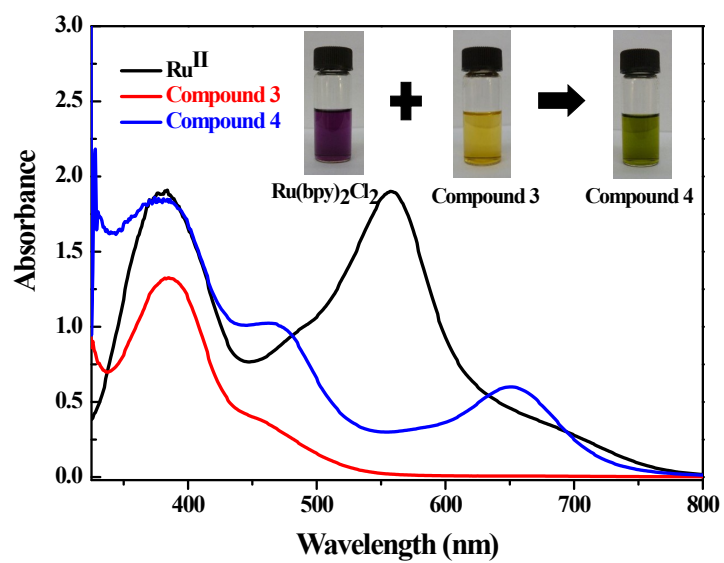


Figure S9 UV-Vis absorption spectra of Compound 2, Compound 3 and their mixture with 1:1 ratio. Conditions: 0.3 mM in acetone/CH₂Cl₂ (1:1, v/v) at 308 K

Table S10. Catalytic oxidation of cyclooctene by Ru(bpy)₂Cl₂ and Al(OTf)₃ in dark.

Entry	Catalyst	Lewis acid	Conversion (%)	Yield (%)
1	-	-	9.7	1.0
2	Ru(bpy) ₂ Cl ₂	-	19.6	7.6
3	-	Al(OTf) ₃	11.5	4.2
4	Ru(bpy) ₂ Cl ₂	Al(OTf) ₃	99.8	90.2

Conditions: acetone/CH₂Cl₂ (4:1, v/v) 1 mL, cyclooctene 0.1 M, *cis*-Ru(bpy)₂Cl₂ catalyst 1 mM, 2,2'-bipyridine 2 mM, Al(OTf)₃ 2 mM, PhI(OAc)₂ 0.2 M, 308 K, 10 h, dark.

Table S11. Catalytic oxidation of cyclooctene by Ru(bpy)₂Cl₂ and Al(OTf)₃ with different oxidant.^a

Entry	Catalyst	Lewis acid	Oxidant	Conversion (%)	Yield (%)
1	-	-	PhIO	5.8	0.4
2	Ru(bpy) ₂ Cl ₂	-	PhIO	14.9	2.1
3	-	Al(OTf) ₃	PhIO	21.3	4.3
4	Ru(bpy) ₂ Cl ₂	Al(OTf) ₃	PhIO	34.0	9.7
5	-	-	H ₂ O ₂	6.5	2.6
6	Ru(bpy) ₂ Cl ₂	-	H ₂ O ₂	9.2	0.5
7	-	Al(OTf) ₃	H ₂ O ₂	16.6	14.0
8	Ru(bpy) ₂ Cl ₂	Al(OTf) ₃	H ₂ O ₂	21.8	18.4
9 ^b	-	-	m-CPBA	87.1	58.1
10 ^b	Ru(bpy) ₂ Cl ₂	-	m-CPBA	92.1	80.8
11 ^b	-	Al(OTf) ₃	m-CPBA	93.4	54.7
12 ^b	Ru(bpy) ₂ Cl ₂	Al(OTf) ₃	m-CPBA	95.1	90.2

Conditions: acetone/CH₂Cl₂ (4:1, v/v) 1 mL, cyclooctene 0.1 M, *cis*-Ru(bpy)₂Cl₂ 1 mM, 2,2'-bipyridine 2 mM, Al(OTf)₃ 2 mM, oxidant 0.2 M, 308 K. [a] 10 h. [b] 3h.

Table S12. Influence of water concentration on the epoxidation of *cis*-stilbene by Ru(bpy)₂Cl₂ and Al(OTf)₃.

Substrate	Water (mL)	Conversion (%)	Yield (%)		
			<i>cis</i> -epoxide	<i>trans</i> -epoxide	benzaldehyde
<i>cis</i> -stilbene	0	74.7	39.1	7.0	15.6
	0.1	78.3	28.7	6.0	36.4
	0.2	59.4	20.1	5.1	18.0

Conditions: acetone/CH₂Cl₂ (4:1, v/v) 1 mL, *cis*-stilbene 0.1 M, *cis*-Ru(bpy)₂Cl₂ 1 mM, 2,2'-bipyridine 2 mM, Al(OTf)₃ 2 mM, PhI(OAc)₂ 0.2 M, 298 K, 12 h.

Table S13. Catalytic oxidation of cyclooctene by Ru(bpy)₂Cl₂ and Al(OTf)₃ under O₂ or Ar^a

Entry	Catalyst	Lewis acid	Oxidant	Conversion (%)	Yield (%)
1	-	-	O ₂	3.9	0
2	Ru(bpy) ₂ Cl ₂	-	O ₂	4.9	0
3	-	Al(OTf) ₃	O ₂	0.7	0
4	Ru(bpy) ₂ Cl ₂	Al(OTf) ₃	O ₂	4.6	0
5 ^b	-	-	PhI(OAc) ₂	14.2	0.5
6 ^b	Ru(bpy) ₂ Cl ₂	-	PhI(OAc) ₂	17.3	4.4
7 ^b	-	Al(OTf) ₃	PhI(OAc) ₂	12.1	1.6
8 ^b	Ru(bpy) ₂ Cl ₂	Al(OTf) ₃	PhI(OAc) ₂	99.7	90.4

Conditions: acetone/CH₂Cl₂ (4:1, v/v) 1 mL, cyclooctene 0.1 M, *cis*-Ru(bpy)₂Cl₂ 1 mM, 2,2'-bipyridine 2 mM, Al(OTf)₃ 2 mM, O₂ balloon, 308 K, 10 h. [b] the reaction was carried out under Ar, PhI(OAc)₂ 0.2 M.